https://doi.org/10.5194/egusphere-2026-4751
Preprint. Discussion started: 13 August 2026

Composite Detection of Continental Shelf Fronts from Sea Surface Temperature and Altimetry: Assessing the Added Value of SWOT KaRIn

Marie-Christin Juhl[1], Marcello Passaro[1], Denise Dettmering[1], Michael Hart-Davis[1], and Martin Saraceno[2,3,4]

[1]Deutsches Geodätisches Forschungsinstitut (DGFI-TUM), Technical University Munich, Germany
[2]Centro de Investigaciones del Mar y la Atmosfera (CIMA/CONICET-UBA)
[3]Departamento de Ciencias de la Atmósfera y los Océanos, Facultad de Ciencias Exactas y Naturales, Universidad de Buenos Aires (DCAO, FCEN-UBA)
[4]Instituto Franco-Argentino para el Estudio del Clima y sus Impactos (IRL 3351 IFAECI/CNRS-IRD-CONICET-UBA)

Correspondence: Marie-Christin Juhl (mariechristin.juhl@tum.de)

Abstract. We present a composite front detection approach that uses horizontal gradients in Absolute Dynamic Topography (ADT) and Sea Surface Temperature (SST) to identify oceanic frontal structures on the Southwestern Continental Atlantic Shelf, a region characterized by strong mesoscale variability and multiple front types. SST fields are derived from the OSTIA satellite product, while four ADT datasets are compared: SWOT MIOST, CMEMS, OK-STv2, and GLORYS12v1. A joint front probability metric is introduced to quantify the co-occurrence of SST- and ADT-derived frontal signatures and to evaluate consistency and differences across products. The method is applied to assess the spatial and seasonal variability of major regional fronts, including the Shelf-Break Front, the San Matías Front, and the Magellan Plume Front. The ADT datasets showed significant differences in their ability to co-detect continental shelf fronts. The Shelf-Break Front was consistently represented across all datasets, with maximum joint front probabilities occurring in austral summer (DJF) and exceeding 96% between 35 and 45°S. In contrast, the seasonal and coastal San Matías Front exhibited stronger dataset dependence, with the highest joint probabilities obtained using SWOT MIOST ADT (73.63%), followed by CMEMS (54.95%), OK-STv2 (41.86%), and GLORYS12v1 (35.16%). In the mid-shelf region (38-41°S), elevated joint frontal probabilities indicate that ADT and SST products, particularly altimetry-based datasets, capture a persistent Mid-Shelf Front. The Magellan Plume Front showed strong joint signatures, most pronounced in SWOT MIOST (97.85%), followed by CMEMS (80.65%), OK-STv2 (72.83%), and GLORYS12v1 (51.09%), with a distinct coastal plume structure during austral winter (JJA). The approach could be further evaluated using ADT from SWOT KaRIn L3 data during SWOT's Cal/val phase, potentially enabling improved detectability through the sharper ADT gradients provided. Overall, the results show that combining SST- and ADT-based gradient detection enhances the characterization of frontal dynamics. The intercomparison further demonstrates that SWOT KaRIn–enhanced gridded altimetry (SWOT MIOST) substantially improves the detection of coastal and seasonal fronts compared with conventional ADT products.

https://doi.org/10.5194/egusphere-2026-4751
Preprint. Discussion started: 13 August 2026

1 Introduction

Frontal systems are key components of continental shelf circulation, separating distinct water masses and generating sharp horizontal gradients in temperature, salinity, and density (Simpson and Hunter, 1974; Brink, 2016; Belkin et al., 2009). Through their influence on the circulation, geostrophic shear, mixing, and water-mass exchange, shelf fronts regulate the transport of heat, nutrients, and carbon across continental shelves and between coastal and open-ocean environments (Huthnance, 1995; Sharples, 2008). As such, accurately resolving shelf fronts is essential for quantifying ocean transport and exchange processes as well as understanding their influence on ecosystem dynamics and biogeochemical cycling.

On the Southwestern Atlantic Continental Shelf (SWACS), previous research (e.g., Rivas and Pisoni, 2010; Acha et al., 2004; Saraceno et al., 2004) identified multiple frontal systems, including the current-induced Shelf-Break Front associated with the boundary currents, estuarine fronts linked to freshwater discharge from the Río de la Plata (∼35°S) and Strait of Magellan (∼52.5°S), as well as mixing fronts connected to stratification and tidal mixing. Belkin (2021) stated that the Patagonian Shelf and shelf break are "unique in the context of the entire World Ocean, since there are no other regions with several prominent year-round fronts", based on a review of frontal regions derived from remote sensing. Studies on the SWACS show that these fronts are driven by distinct processes but are commonly characterized by strong horizontal gradients in, e.g., Sea Surface Temperature (SST), Sea Surface Salinity (SSS), and Ocean Color (OC) (e.g., Pisoni et al., 2015; Rivas, 2006)).

Front detection has evolved from manual interpretation of SST imagery to increasingly sophisticated automated approaches, including the histogram-based edge-detection algorithm of Cayula and Cornillon (1992), gradient-based operators such as Sobel and Canny filters (Nieto et al., 2012), and SSH-derived geostrophic methods based on satellite altimetry that are largely insensitive to cloud contamination (Sokolov and Rintoul, 2009). The core limitation of single-image detection, namely incomplete spatial coverage caused by persistent cloud cover, motivated the first composite front detection approaches, in which Cayula and Cornillon (1992) and later Belkin et al. (2009) aggregated binary front detections from multiple satellite passes into frontal probability maps, establishing the basic framework for frontal climatologies. Subsequent composite approaches diversified considerably, including maximum-gradient compositing methods that preserve peak thermal signatures across image stacks, multi-sensor compositing approaches designed to improve spatiotemporal coverage, altimetry-based frontal tracking using Sea Surface Height (SSH) contours (Sokolov and Rintoul, 2009; Chambers, 2018), and biophysical compositing methods combining SST and chlorophyll-*a* fronts to characterize coupled thermal and biological frontal structures (Wang et al., 2021; Miller, 2009; Belkin et al., 2009).

SST fronts can coincide with topographic gradients, seen as slopes in SSH or in the Absolute Dynamic Topography (ADT), which is directly linked to geostrophic circulation. This can occur when both reflect the same underlying density structure and a geostrophically balanced circulation, where horizontal density gradients generate pressure gradients and associated surface geostrophic flow. In such cases, SST fronts may exhibit clear ADT signatures, while dynamically driven fronts identified from altimetry can conversely imprint on SST through advection, stirring, and mixing processes (e.g., Belkin et al., 2009; Graham, 2013; Saraceno et al., 2014). However, not all thermal fronts are dynamically controlled, as SST patterns can also be shaped by air–sea heat fluxes, freshwater input, and vertical mixing, producing thermal fronts with weak or absent ADT

https://doi.org/10.5194/egusphere-2026-4751
Preprint. Discussion started: 13 August 2026

signatures, particularly in shallow shelf and coastal environments (Simpson and Hunter, 1974; Simpson and Sharples, 2012). Accordingly, most existing front detection approaches rely on either SST (e.g., Cayula and Cornillon, 1992; Belkin et al., 2009) or SSH independently (Sokolov and Rintoul, 2009; Graham, 2013), or compare the resulting fronts a posteriori, rather than exploiting their joint dynamical relationship. This motivates a combined SST-ADT framework that identifies fronts associated with dynamically resolved frontal structures. At the same time, it provides a robust basis for assessing the ability to detect continental shelf fronts from observational sea-level maps.

However, assessing the correspondence between SST fronts and dynamically resolved frontal structures remains challenging because the spatial scales effectively resolved by gridded sea level products based on satellite altimetry are substantially larger than their nominal grid spacing. Typical spatial effective resolutions of altimetry-derived products are in the range of hundreds of kilometers, depending on the region and mapping product (Ballarotta et al., 2019), with a lack of energy on sub-annual scales reported on the SWACS (Juhl et al., 2024). Consequently, submesoscale fronts and filaments are generally not resolved, as demonstrated in Antarctic Circumpolar Current fronts by Siegelman et al. (2020). Recent advances in mapping methodologies, including the Multiscale Inversion of Ocean Surface Topography (MIOST) technique (Ubelmann et al., 2021a, b), have improved the representation of mesoscale variability, although fundamental resolution limitations remain. The recent Surface Water and Ocean Topography (SWOT) mission represents a major advance by providing wide two-dimensional observations of the sea surface, enabling a new generation of gridded products with improved capability for resolving mesoscale (Verger-Miralles et al., 2025; Archer et al., 2025) and coastal dynamics, including coastal-trapped waves (Poli et al., 2025; Passaro, 2025).

Despite advances in satellite altimetry, the ability of gridded products to resolve continental shelf fronts remains uncertain, particularly in complex coastal regions. Here, we assess whether using daily sea level maps generated from both nadir-only altimetry missions and wide-swath observations (which we call here SWOT-enhanced gridded altimetry for simplicity) improves shelf-front detection relative to conventional altimetry products and model-derived fields using a composite SST-ADT front-detection framework. Using the SWACS frontal system as a test bed, we examine which front types exhibit detectable ADT signatures and how consistently they are resolved across datasets. This framework also enables a critical assessment of gridded altimetry in coastal regions and the added value of SWOT KaRIn data. Specifically, we ask: (1) To what extent can nadir-only and SWOT-enhanced gridded altimetry resolve continental shelf fronts? (2) Which front classes exhibit detectable ADT signatures across datasets?

https://doi.org/10.5194/egusphere-2026-4751
Preprint. Discussion started: 13 August 2026

2 Data and Methods

2.1 Data

2.1.1 Gridded altimetry

Altimetry-based Absolute Dynamic Topography (ADT) used in this study is obtained from the following products:

- CMEMS: The operational global gridded ADT product distributed by the Copernicus Marine Service. It combines observations from multiple nadir altimeter missions and reconstructs the sea surface using the Multiscale Inversion of Ocean Surface Topography (MIOST) technique (Ubelmann et al., 2021a, b).

- SWOT MIOST: An experimental extension of the CMEMS MIOST product that additionally incorporates wide-swath observations from the Science phase of the Surface Water and Ocean Topography (SWOT) mission. The enhanced spatial coverage improves the representation of mesoscale variability and coastal dynamics (Archer et al., 2025).

- OK-STv2: A regional gridded ADT product generated using spatio-temporal window kriging within the continental shelf (Juhl et al., 2025, 2026). The gridded data are derived from along-track altimeter observations provided by CMEMS and are publicly available through SEANOE (https://doi.org/10.17882/103947)

All datasets are provided on their native grids with a spatial resolution of 0.125° and daily temporal resolution. We use the time period from 31st July 2023 to 1st August 2024 at 0.125° resolution, beginning with the first month of availability of the SWOT-enhanced MIOST product. In a comparison to the SWOT KaRIn data in Section 4.6, we use the SWOT MIOST dataset within the SWOT Cal/Val phase instead of the Science phase. ADT is defined as the sum of Sea Level Anomaly (SLA) and Mean Dynamic Topography (MDT), from which surface geostrophic velocities can be derived. The SLA fields are corrected for tides using the FES 2022 tidal model and for atmospheric effects using the Dynamic Atmospheric Correction (DAC).

2.1.2 SWOT KaRIn

Additionally, the SWOT KaRIn L3 Expert product v3.0 data are used within the Cal/val phase from March to July 2024 to test the composite front detection on the wide-swath using track #007 that crosses most of the study region during the Cal/val phase with a daily frequency. We use the ADT from the sum of the filtered SSH and the MDT given in the product.

2.1.3 Model

In addition, we use the model reanalysis GLORYS12v1, which is based on the NEMO ocean model. It uses, among others, assimilation of along-track SLA observations from all nadir altimetry missions and is thus not completely independent of gridded altimetry. The original spatial resolution of 1/12° was reduced to 1/8° through spatial averaging to match the resolution of the gridded altimetry products, while preserving the model's daily temporal resolution. The model provides sea surface height above the geoid ("zos"), referenced to the static EGM96 geoid. Although the altimetric products use different geoid

https://doi.org/10.5194/egusphere-2026-4751
Preprint. Discussion started: 13 August 2026

models (e.g., GOCO06S in the SWOT MIOST product), the model-derived sea surface height is dynamically comparable to the ADT derived from satellite altimetry and is, therefore, referred to hereafter as ADT. These model-derived ADT fields do not include tides or the inverse barometer effect and consequently do not require the corresponding corrections applied to altimetric observations. Juhl et al. (2024) showed that the model has a stronger correlation with tide gauges in SWACS than with CMEMS gridded altimetry.

2.1.4 Sea Surface Temperature

SST fields were obtained from the Operational Sea Surface Temperature and Ice Analysis (OSTIA), distributed publicly available by the Copernicus Marine Service. OSTIA provides a global, gap-free Level-4 analysis at 0.05° spatial resolution by combining infrared and microwave satellite observations with in-situ measurements using optimal interpolation (OI). Due to the spatial correlation scales of OI (∼10km), the effective resolution is coarser than the nominal grid (Donlon et al., 2012). This scale is comparable to the effective resolution of sea surface height fields from SWOT after noise filtering (∼15–30 km; e.g., Fu et al. (2023)), making the dataset suitable for combined frontal analyses, as both SST and altimetric gradients consistently resolve mesoscale features while suppressing smaller-scale noise.

2.2 Methods

2.2.1 Geostrophic Velocities

From the ADT of the model and altimetry datasets, we derived the geostrophic velocities by applying the geostrophic relation using the following equations defined on latitudes y and longitudes x:

$$u_g = \frac{-g}{f(y)} \cdot \frac{\partial ADT}{\partial y} \tag{1}$$

$$v_g = \frac{g}{f(y)} \cdot \frac{\partial ADT}{\partial x} \tag{2}$$

with the acceleration of gravity g, the Coriolis parameter f at the latitude y, and the distance of two points ∂x, ∂y in m.

2.2.2 Composite Front Detection from SST and ADT

Below, the composite front detection method is explained, including the computation of horizontal gradients, front thresholding, and the computation of the joint front probability, which will be analyzed as the final result. The schematic in Figure 1 gives an overview of these steps, explained below:

https://doi.org/10.5194/egusphere-2026-4751
Preprint. Discussion started: 13 August 2026

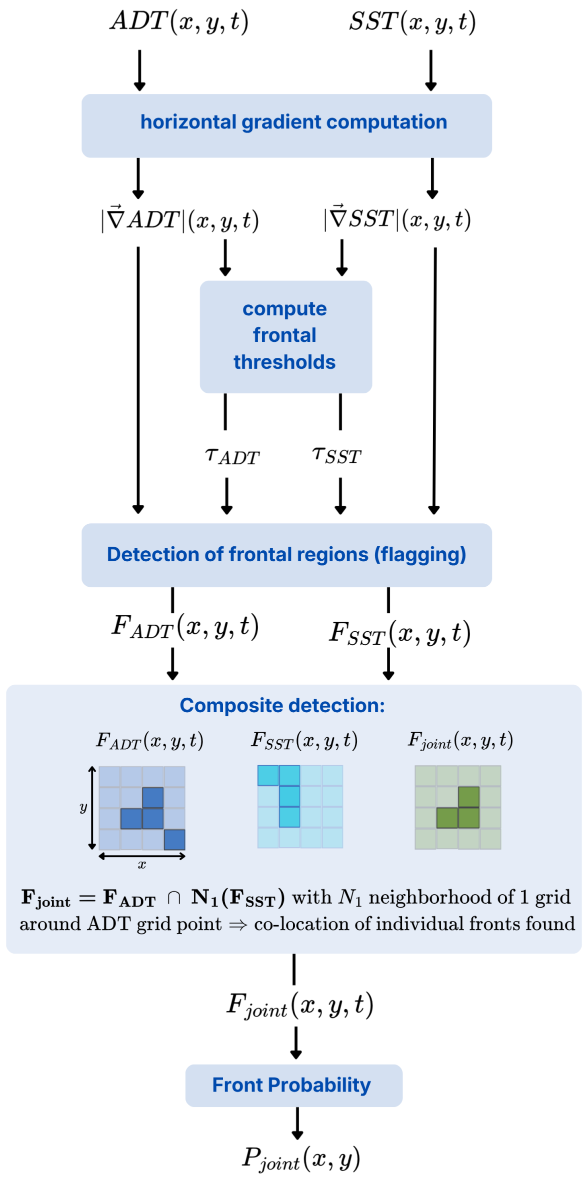

Figure 1. Workflow of composite front detection method from Sea Surface Temperature (SST) and Absolute Dynamic Topography (ADT) using thresholds (τ_{SST} and τ_{ADT}) resulting in a joint front probability (P_{joint}).

Horizontal gradients

We built on several previous studies that analyze frontal regions using horizontal gradients: We compute them from ADT and SST separately, as stated in the following equation:

$$|\nabla ADT| = \sqrt{\left(\frac{\partial ADT}{\partial x}\right)^2 + \left(\frac{\partial ADT}{\partial y}\right)^2} \quad \text{and} \quad |\nabla SST| = \sqrt{\left(\frac{\partial SST}{\partial x}\right)^2 + \left(\frac{\partial SST}{\partial y}\right)^2} \tag{3}$$

where x and y are referring again to longitude and latitude. The resulting horizontal gradients are expressed thus in units of m km^{-1} and °C km^{-1}, respectively. Horizontal gradients are thus obtained per grid point, except for cropped points at the edges (e.g., along the coast) due to derivatives, retaining the resolution of the gridded dataset at daily and 0.125°.

Threshold of fronts from horizontal gradients

Front detection was performed by applying a percentile-based threshold to the horizontal gradient magnitude, retaining only pixels exceeding the upper tail of the gradient distribution, following the common definition of fronts as regions of enhanced gradients (e.g., Canny, 2009). Thresholds were set to the 95th percentile for SST (τ_{SST}) and the 80th percentile for ADT (τ_{ADT}). A lower threshold was adopted for ADT because altimetry-derived gradients exhibit a narrower dynamic range than SST gradients due to the effective smoothing inherent in mapped ADT products. A 95th-percentile threshold yielded overly sparse detections and failed to capture spatially coherent frontal structures. Sensitivity tests using τ_{ADT} values between the 70th and 95th percentiles (Supplementary Fig. B1) showed that the main frontal patterns are robust to threshold choice. The 70th percentile has previously been used for SSH-based front detection (Sudre et al., 2023). Thresholds were computed separately for each dataset, allowing the method to adapt to differences in resolution, noise characteristics, and gradient distributions. Based on τ_{ADT} and τ_{SST}, frontal masks were defined as follows:

$$F_{\mathrm{ADT}}(t,\mathbf{x}) = \begin{cases} 1, & |\nabla ADT| > \tau_{ADT}, \\ 0, & |\nabla ADT| \leq \tau_{\mathrm{ADT}}. \end{cases} \quad \text{and} \quad F_{\mathrm{SST}}(t,\mathbf{x}) = \begin{cases} 1, & |\nabla SST| > \tau_{SST}, \\ 0, & |\nabla SST| \leq \tau_{\mathrm{SST}}. \end{cases} \tag{4}$$

The detection in Equation 4 produces a binary mask over time and the analyzed grid, where 1 indicates a detected front, and 0 indicates no front.

Composite detection

To identify fronts detected in both SST and ADT, we combine the binary frontal masks to a joint frontal mask F_{joint}, while allowing for small spatial offsets arising from differences in resolution, geostrophic adjustment, and advection. Using the individual frontal masks F_{ADT} and F_{SST} derived from ADT and SST, the joint frontal mask F_{joint} is defined as:

$$F_{\mathrm{joint}}(x,y,t) = F_{\mathrm{ADT}}(x,y,t) \cap N_r(F_{\mathrm{SST}}(x,y,t)) \tag{5}$$

https://doi.org/10.5194/egusphere-2026-4751
Preprint. Discussion started: 13 August 2026

where $N_r(F_{\mathrm{SST}})$ denotes the SST frontal mask dilated by a neighborhood of radius (r) grid cells. Thus, an ADT frontal pixel is classified as a joint front if at least one SST frontal pixel occurs within its neighborhood. This accounts for small spatial displacements between thermal and dynamical frontal signatures while preserving their co-location.

This asymmetric definition is centered on ADT to identify SST fronts with a dynamical signature in dynamic height, i.e., fronts consistent with geostrophic structure. We set $r = 1$ grid points of the altimetric product ($0.125°$), corresponding to ~ 10–$15\,\mathrm{km}$. Sensitivity tests with $r = 1$–3 grid points yield qualitatively similar results, indicating robustness, but higher r values result in smearing of frontal shapes (not shown). The approach can be compared to convolving the single pixels with a Gaussian filter in the SST mask prior to intersection, as in Miller (2009), and accounts for spatial offsets arising from differences in resolution, geostrophic adjustment, and advection.

Joint front probability

The probability of composite-detected fronts is computed using a probability function that quantifies the persistence of frontal regions at each grid point, based on the individually detected fronts for each day. Probability is defined as:

$$P_{\mathrm{joint}}(\mathbf{x}) = \frac{1}{T}\sum_{t=1}^{T} F_{joint}(t,\mathbf{x}). \tag{6}$$

with T, the total length of time. Thus P_{joint} will be a value between 0 and 1, with 1 (0) being joint frontal occurrence in each of all (none) days analyzed.

3 Study Region

Our study region is the Southwestern Atlantic Continental Shelf (SWACS) between 30° and 55°S and within 40° and 70°W. The continental shelf is restricted by the 200m-isobath, marking the inner shelf break towards the open ocean (Figure 2). The circulation on the SWACS is influenced by the western boundary currents outside the shelf break, primarily by the Malvinas Current (MC), which transports cold water from the Antarctic Circumpolar Current (ACC) northward along following the bathymetry of the outer shelf break (Fig. 2). Near 41°S, the Malvinas Current is known to have inflows onto the shelf, directly impacting shelf circulation (Piola et al., 2010). The Malvinas Current meets the warm southward-flowing Brazil Current (BC) at approximately 34-36°S, forming the Brazil-Malvinas Confluence, one of the most energetic regions in the world's oceans. On the continental shelf, mean circulation reflects the off-shelf flow, with southward Brazil shelf waters flowing south till ∼36°S and northward cold water from ACC intrusions in the south flowing northward.

The coastal circulation is influenced by the discharge of major rivers, including the Río de la Plata (∼35°S) and the Strait of Magellan (∼53°S), where fronts form from the river plumes intruding the continental shelf waters. The coastline exhibits complex geomorphological features, such as the San Matías Gulf (SM), where tidally mixed waters form in austral summer, creating the San Matías front at the gulf's exit upon meeting shelf water, stratified by ocean surface heat flux.

https://doi.org/10.5194/egusphere-2026-4751
Preprint. Discussion started: 13 August 2026

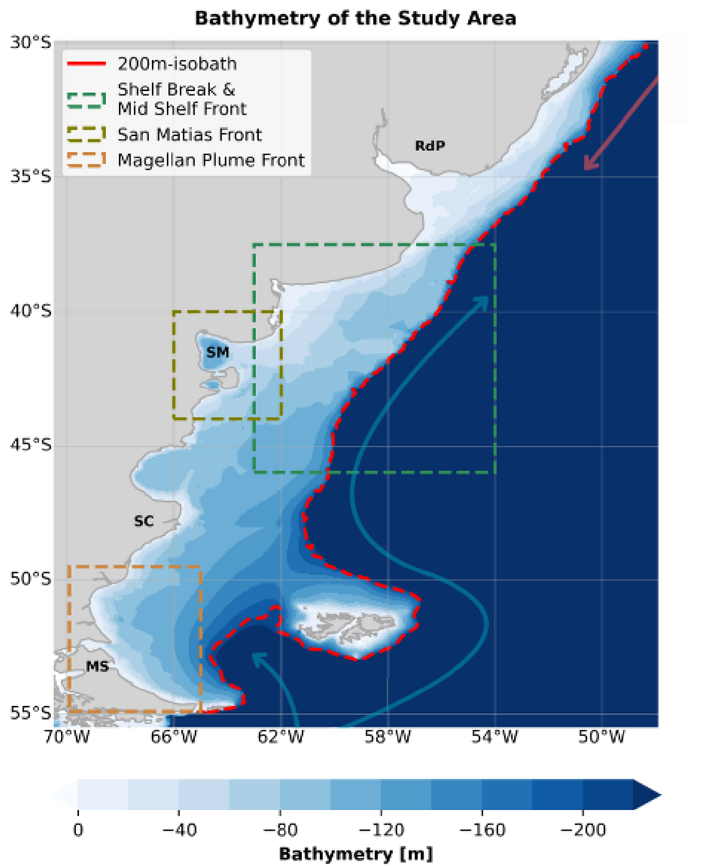

Figure 2. Bathymetry of the Study region and Subregions highlighted in the study. Marked are the Río de la Plata estuary (RdP), San Matías gulf (SM), Santa Cruz area (SC), and the Magellan Strait (MS). The 200m-isobath marks the shelf break (red dashed line), while off the shelf, the western boundary currents, the Malvinas Current (blue arrow) and the Brazil Current (red arrow), are drawn schematically.

https://doi.org/10.5194/egusphere-2026-4751
Preprint. Discussion started: 13 August 2026

4 Results and Discussion

During the composite front detection, elevated joint front probabilities coincide with previously documented frontal systems on the SWACS, although the ability to resolve individual fronts varies among the datasets, resulting in robust detection of some frontal systems while others are only partially resolved (Rivas and Pisoni, 2010; Acha et al., 2004; Saraceno et al., 2004). In contrast, considering SST fronts alone (i.e., horizontal SST gradients exceeding the selected threshold) reveals additional frontal features that are not identified by the composite approach because no corresponding ADT front is detected. These features are briefly discussed in Section 4.5. In the following, we first examine the quasi-permanent Shelf-Break Front, followed by selected coastal and seasonal fronts, including tidal mixing fronts and freshwater plume-related fronts.

The mean joint frontal probability fields over the study period (Figure 3) consistently identify the major frontal systems of the SWACS. The Shelf-Break Front (A), extending between approximately 35°S and 45°S, is clearly detected in all ADT datasets, demonstrating that this large-scale frontal system is robustly identified irrespective of the underlying altimetry product. Elevated joint frontal probabilities are also observed in the Río de la Plata plume region (B), consistent with known plume-induced density gradients and associated frontal circulation. Additional regions of enhanced frontal probability occur in the El Rincón estuary (D), at the mouth of San Matías Gulf (E), and on both sides of the Strait of Magellan (F), corresponding to the Magellan plume and Tierra del Fuego tidal front. Overall, the detected frontal regions closely coincide with previously documented oceanographic fronts, indicating that the composite detection predominantly identifies physically meaningful frontal structures rather than producing widespread false detections.

We first analyze the joint front probability (P_{joint}) along the Shelf-Break Front. Owing to its quasi-permanent nature and its close association with the shelf-break bathymetry, the front can be sampled by extracting the grid cells nearest to the 200 m isobath (see Figure 2). This provides a consistent reference for comparing frontal probabilities among the different datasets along the full extent of the shelf break.

https://doi.org/10.5194/egusphere-2026-4751
Preprint. Discussion started: 13 August 2026

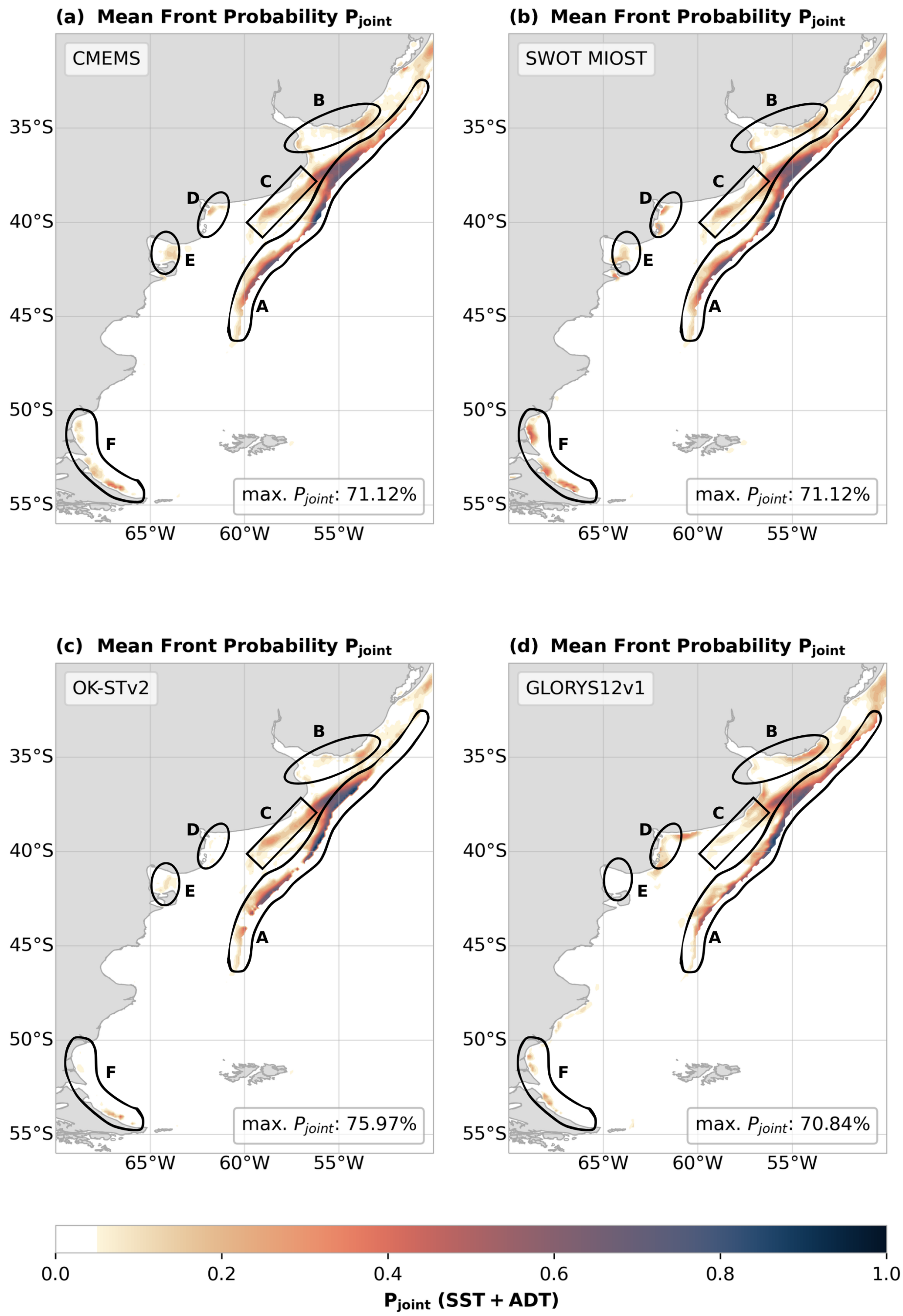

Figure 3. Annual mean Front Probability P_{joint} on the SWACS for ADT from different gridded altimetry products. Frontal regions highlighted: Shelf-Break Front (A), Río de la Plata plume front (B), Mid-shelf Front (C), El Rincón Estuarine Front (D), San Matías Front (E), and Tierra del Fuego tidal front connected to Magellan plume (F).

https://doi.org/10.5194/egusphere-2026-4751
Preprint. Discussion started: 13 August 2026

4.1 The Shelf-Break Front

For all altimetry datasets and the numerical model used in the composite front detection, the Shelf-Break Front is clearly identified as a front with high P_{joint} values and is consistent with the known position between 35° and 45°S of this front being dominant, as reported previously (Saraceno et al., 2004; Franco et al., 2017). The joint front probability for the Shelf-Break Front is consistently significant at these latitudes across the ADT datasets, reaching >96% in the austral summer (DJF) between 35 and 45°S (Figure 4).

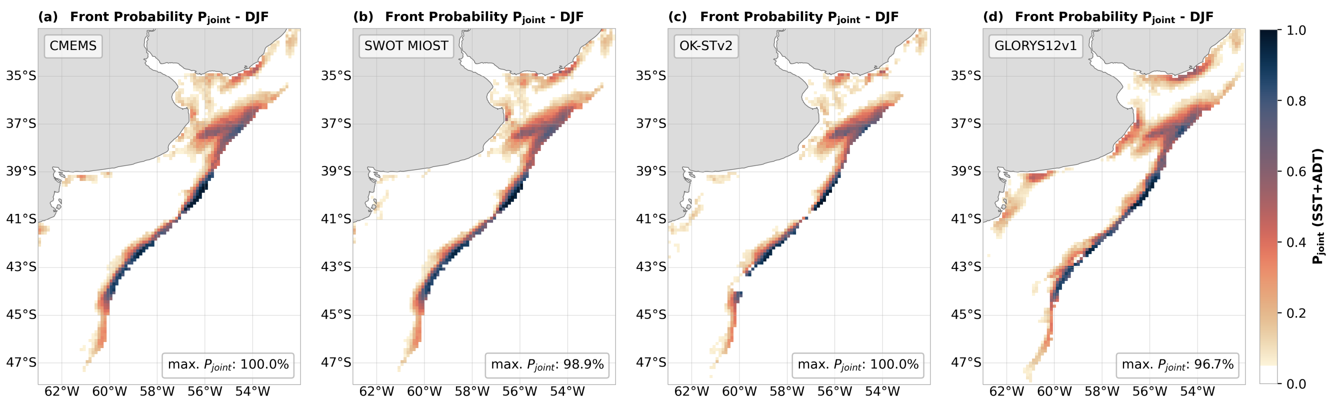

Figure 4. Joint front probability P_{joint} at the Shelf-Break Front in different seasons from composite front detection using SST and ADT from different datasets. Values from the continental shelf (outside the 200-m isobath) are not shown.

In contrast to the enhanced frontal signal during austral summer, characterized by elevated joint front probabilities in DJF, the Shelf-Break Front exhibits a reduced detectability during austral winter (Figure 5). South of approximately °S, joint front probabilities decrease to near zero during winter in all datasets. This reduction is likely related to the seasonal cooling of shelf waters, which reduces the contrast in SST between the SWACS and the cold Malvinas Current, thereby weakening the cross-front SST gradient (see Appendix D1). Consequently, the SST signature of the Shelf-Break Front becomes insufficient for detection in the southern part of the front during winter. Conversely, increased joint front probabilities are observed north of 36°S from autumn to spring, suggesting a seasonal northward displacement of the detectable frontal signal. This pattern may be linked to the seasonal variability of the regional western boundary current, which exhibits a latitudinal shift of approximately 1.5° for the northern front, associated with seasonal changes in transport of e.g., the Brazil Current (Artana et al., 2019). These seasonal variations in strength and location contribute to the joint front probabilities remaining below 100% in the annual mean (Figure 4), despite the Shelf-Break Front being a persistent hydrographic feature of the region.

https://doi.org/10.5194/egusphere-2026-4751
Preprint. Discussion started: 13 August 2026

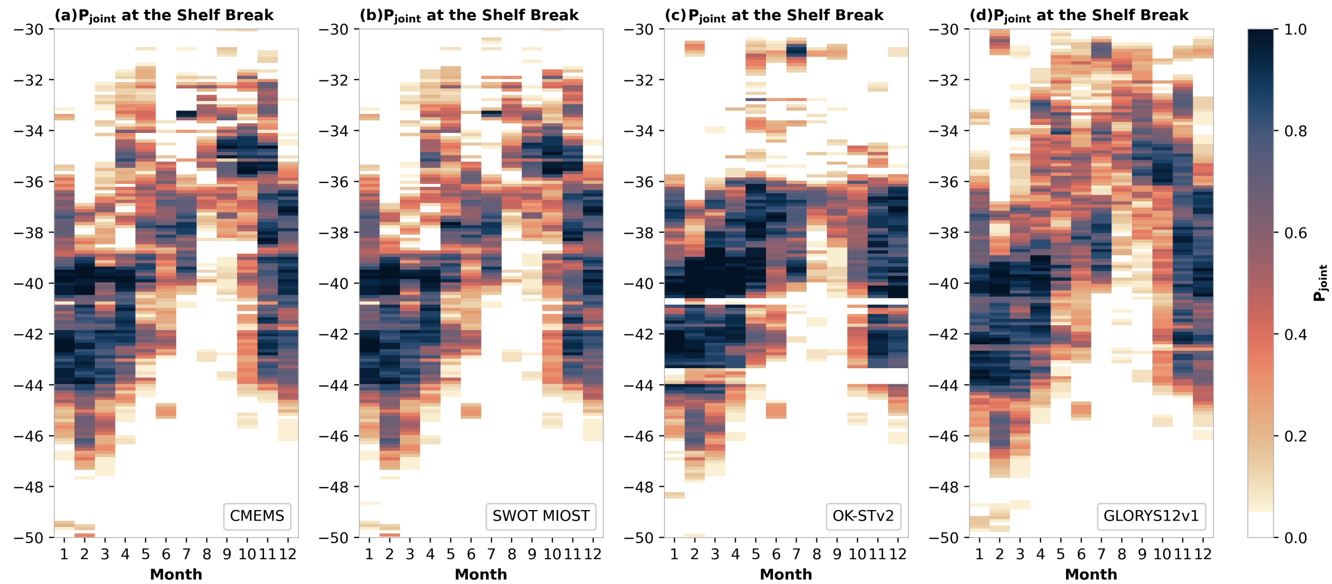

Figure 5. Joint front probability P_{joint} extracted along the Shelf Break (200m-isobath) for ADT from different gridded altimetry products across different months and latitudes.

4.2 Seasonal and coastal Fronts

Inspecting the joint frontal probabilities for each season separately, distinct SST-ADT fronts appear, as evidenced by an increase in P_{joint} in the composite approach, since many fronts underly seasonality. Here, we highlight the ocean front in the mouth of the San Matías Gulf, a coastal region that is particularly challenging to study from altimetry and model data due to the complex coastline and the macrotidal character of the region (Barclay et al., 2023; Hart-Davis et al., 2026). In Figure 6, P_{joint} is shown for all four seasons using the ADT from the SWOT MIOST dataset. In the San Matías Gulf, values of up to 73.63% occur near the gulf mouth (41.5°S, 64°W) during DJF. This feature corresponds to the San Matías Front, previously identified from high-resolution SST observations by Rivas and Pisoni (2010). The front develops during the austral summer as enhanced surface heating promotes stratification, while strong tidal mixing persists in the northeastern gulf, creating a sharp boundary between stratified and mixed waters. As a result, the front is a seasonal feature evident only during DJF.

https://doi.org/10.5194/egusphere-2026-4751
Preprint. Discussion started: 13 August 2026

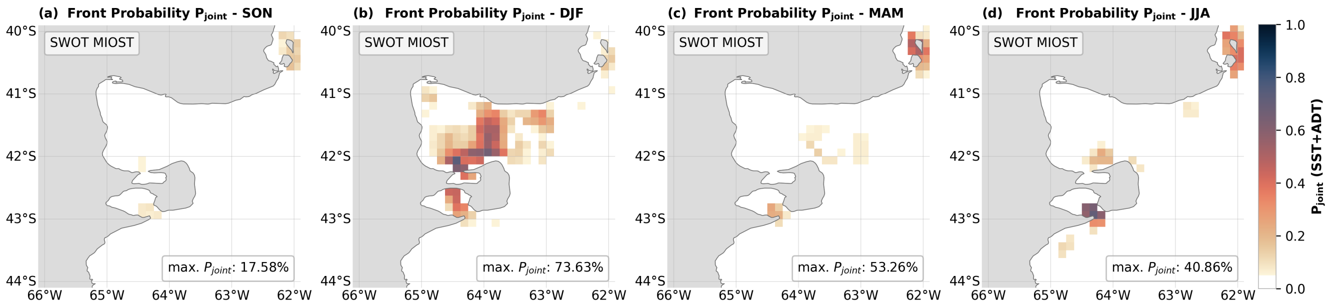

Figure 6. Joint front probability P_{joint} at the San Matías gulf in different seasons from composite front detection using SST and altimetry-based ADT from SWOT MIOST.

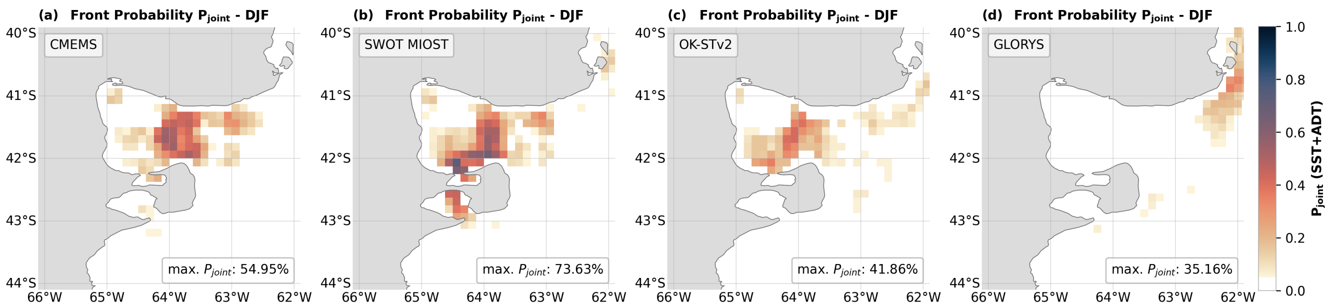

Figure 7. Joint front probability P_{joint} at the San Matías gulf from composite front detection in DJF using SST and ADT from different datasets.

The ADT-sensitive component of the mixing front cannot be unambiguously linked to a specific dynamical mechanism, as causality cannot be inferred from the composite front detection alone. Nevertheless, the elevated horizontal ADT gradients are consistent with the presence of a cross-front density gradient. Such density contrasts can generate sea-surface height gradients through geostrophic adjustment, producing a detectable signal in ADT. The ADT expression of the front, therefore, likely represents the baroclinic structure associated with the boundary between stratified and tidally mixed waters.

In Figure 7, we highlight the DJF season in which the San Matías Front is present. Across all datasets, the SWOT MIOST dataset clearly achieves the highest joint front probability P_{joint} (73.63%). Despite the grid resolution of 0.125° (∼14km), the front shape crossing the mouth of the gulf is recognizable. Also, CMEMS and OK-STv2 capture the pattern of the front, however, with lower P_{joint} values of 54.95% and 41.86%, respectively. GLORYS12v1 does not capture the San Matías front, most likely because the underlying mechanism, tidal mixing, is not explicitly resolved or is effectively weakened in the reanalysis framework, since tidal processes are not fully represented.

https://doi.org/10.5194/egusphere-2026-4751
Preprint. Discussion started: 13 August 2026

4.3 Mid Shelf Front

The composite SST+ADT front detection reveals a distinct frontal feature in the middle of the northern Patagonian shelf, during MAM (austral autumn), situated at approximately 38–40°S and located well inshore of the Shelf-Break front and clearly seperated from the shelf break, exhibiting the highest P_{joint} values of any feature in this subregion (Figure 8, black rectangle). This front appears prominently across all four ADT datasets, though with considerable variability in maximum P_{joint}. Notably, the front is identifiable across all seasons, as seen in monthly mean ADT horizontal gradients above threshold (Figure C2), whereas the joint front probability peaks strongly in MAM, suggesting that the thermal expression of the front is coherent only with the dynamic height gradient during the austral autumn.

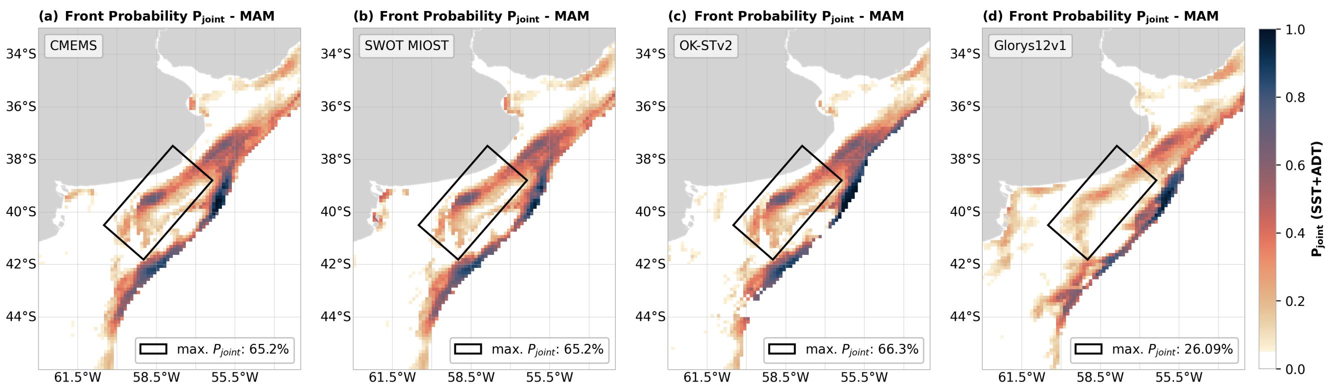

Figure 8. Joint front probability P_{joint} at the Mid Shelf Front from composite front detection in MAM using SST and ADT from different datasets.

In Figure 9, we show the ADT and derived geostrophic velocities for the MAM season in the regions, while inspecting a cross-shelf transect (red dashed line), which also crosses the front. The transect co-occurs at the same location as a sharp maximum in P_{joint} approximately 100 km from the coast in all datasets except GLORYS12v1, which shows a systematically lower and broader signal. The altimetry-based ADT fields (Figure 9) consistently reveal a band of enhanced dynamic height gradient seen by the derived geostrophic velocities (see Eq. 1, 2) in this mid-shelf position, oriented parallel to the coast and aligned with the frontal corridor identified in the probabilistic maps. These gradients give rise to enhanced geostrophic velocities in the mid-shelf, which remain embedded within the general northward mean flow.

https://doi.org/10.5194/egusphere-2026-4751
Preprint. Discussion started: 13 August 2026

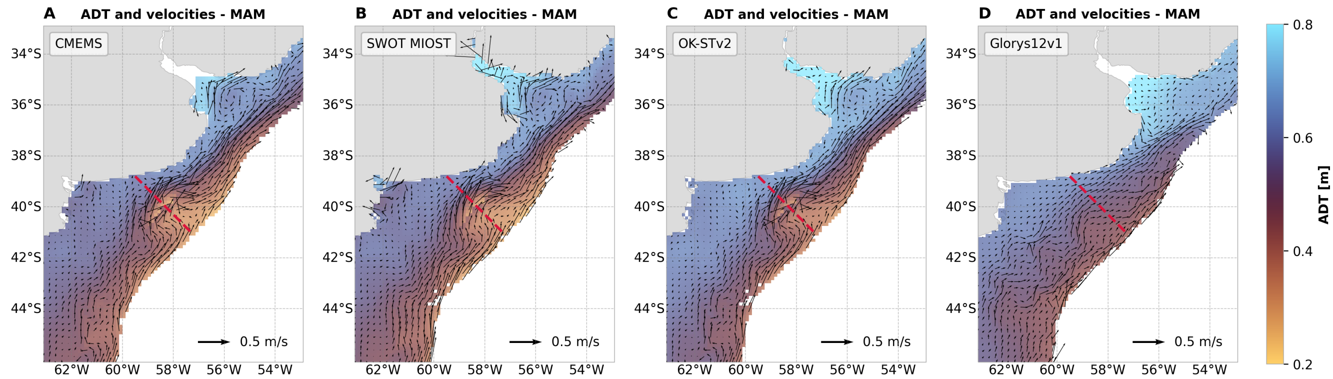

Figure 9. Geostrophic velocities in MAM around the Mid Shelf Front from different ADT datasets. The red dashed line marks the cross-front transect.

The frontal feature identified here corresponds to the Mid-Shelf Front (MSF) of the northern Patagonian shelf, a dynamically complex and biologically significant boundary that has been the subject of increasing attention in the literature. The MSF can be found off the coast of the El Rincón region (approximately 39–41°S), where the coastal-inner shelf area is shaped by retention processes and the interaction of distinct water masses (Lucas et al., 2005). Rivas and Pisoni (2010) were among the first to systematically document frontal pixels in this area using satellite SST climatologies, noting their recurrent occurrence, though without conclusively attributing them to a single mechanism. Subsequently, Marrari et al. (2013) formally named and characterized this boundary as the Mid-Shelf Front, describing it as a chlorophyll-defined front associated with the confluence of distinct water-mass populations and identified as a habitat boundary for commercially important species. Strub et al. (2015) reported jet-like behavior in the geostrophic velocities in the mid-shelf, while Ruiz Etcheverry et al. (2016) documented a rapid velocity gradient across a cross-shelf transect near 39.87°S, with geostrophic velocities increasing from near-zero inshore to approximately 20 cm/s toward the shelf-break, showing stronger gradients in late summer and autumn.

The combined SST and ADT signature of the MSF, particularly pronounced during MAM, reflects the thermohaline contrast between warm, saline waters exported from the San Matías Gulf and the cooler, fresher mid-shelf waters of the Patagonian Current system (Lucas et al., 2005; Rivas and Pisoni, 2010). This water mass boundary generates both a strong thermal gradient, as observed in SST, and a steric SSH gradient that is detectable in ADT. The resulting cross-front density contrast is associated with a geostrophic SSH gradient that supports the along-front geostrophic jet described by Strub et al. (2015) and Ruiz Etcheverry et al. (2016). The persistent ADT gradient suggests a quasi-permanent geostrophic jet associated with the MSF. In addition to the density-driven pressure gradient across the front, regional convergence of isobaths may contribute to topographic steering and intensify the northward flow. However, the circulation is primarily controlled by alongshore wind forcing (Lago et al., 2019, 2021). The persistent ADT signal suggests that the geostrophic structure of the MSF is maintained throughout the year, whereas the SST expression is seasonally enhanced during MAM, when thermal contrasts across the front become more pronounced. Consequently, the joint SST–ADT detection is strongest during this season.

https://doi.org/10.5194/egusphere-2026-4751
Preprint. Discussion started: 13 August 2026

4.4 River Plume Fronts

The SWACS is strongly influenced by freshwater inputs from, e.g., the Río de la Plata, the El Rincón estuary region, and the Strait of Magellan. These fluxes are generating buoyant plumes that are readily observed in ocean color and SST data due to strong density gradients and, in the case of the Río de la Plata, high suspended sediment concentrations (Piola et al., 2005; Burrage et al., 2008).

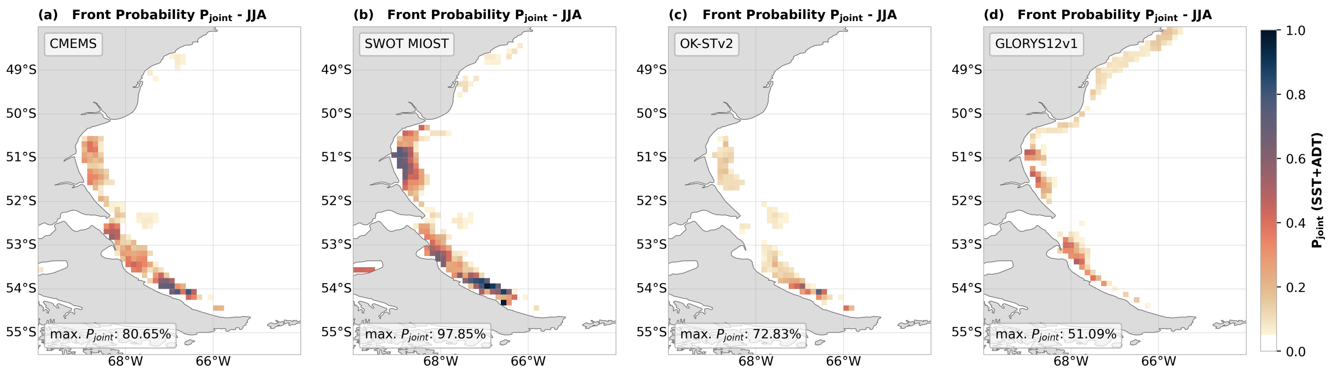

Figure 10. Joint front probability P_{joint} at the Magellan Plume Front from composite front detection in JJA using SST from OSTIA and ADT from different datasets.

The joint front probability (P_{joint}) during JJA reveals a persistent region of elevated frontal activity at the eastern entrance of the Strait of Magellan and the adjacent shelf, with notable differences in magnitude and spatial extent among the datasets (Figure 10). All datasets indicate that enhanced joint front occurrence is not confined to the immediate coastal plume. Instead, the Magellan plume is known to be transported predominantly northward from the Atlantic entrance of the Strait of Magellan, while enhanced frontal activities extended to the south of the Strait likely reflect the persistent Tierra del Fuego Front associated with water exchange through the Le Maire Strait and interactions between subantarctic shelf waters and the freshwater outflows. The front is known to have a semi-annual cycle in SST (see Rivas and Pisoni (2010), Fig. 7), while we find the highest P_{joint} in agreement with this occurring during JJA, coinciding with the season of strongest northwards shelf transport, driven by enhanced wind forcing and macrotidal mixing. This increased transport extends the frontal signature both northward along the coast and farther offshore onto the inner shelf.

All four products agree that the primary frontal corridor on both sides of the Magellan Strait coincides with the region where subantarctic shelf waters interact with the Strait outflow. However, the maximum P_{joint} values differ substantially: GLORYS12v1 yields the most conservative estimate with 51.09%, followed by OK-STv2 (72.83%) and CMEMS (80.65%), while SWOT MIOST again produces by far the highest frontal probabilities, reaching 97.85% and exhibiting a markedly broader and more intense frontal zone, particularly along the southern shelf edge near 54–55°S. The persistent frontal corridor detected across all four datasets along the eastern entrance of the Strait of Magellan and the adjacent shelf is consistent with the well-documented mixing front described in the literature (Acha et al., 2004; Rivas and Pisoni, 2010). This front is associated with strong gradients arising from the exchange of cold, low-salinity subantarctic waters through the Strait of Magellan as well as water inflow through the Le Maire Strait further to the east, and their mixing caused by winds and tides with adjacent shelf waters. Knowing that, we infer that the front is not purely thermal but likely involves a co-located density gradient that is seen in both SST and ADT. The low-salinity core waters exiting the Atlantic mouth of the Strait are known to create a strong baroclinic signal that drives intense eastward geostrophic velocities and a net Pacific-to-Atlantic transport. The strong salinity gradient at the front (Brun et al., 2020) indicates a baroclinic pressure field that, under geostrophic balance, is associated with surface geostrophic currents and corresponding sea surface height gradients potentially observable in ADT.

The Magellan Plume is fundamentally buoyancy-driven, with its structure set by horizontal density gradients associated with the freshwater salinity anomaly and modified by rotation and ambient shelf circulation (Palma and Matano, 2012). These density gradients imply a baroclinic pressure field in approximate geostrophic balance, which is associated with a slight elevation of the sea surface over the fresher side of the plume front relative to the surrounding denser subantarctic shelf waters. In principle, this steric (primarily halosteric) contribution can generate weak sea surface height gradients that may be reflected in ADT, although such signals are typically small and difficult to resolve near coastal boundaries. However, the detectability of this ADT signal is critically dependent on the ADT product's spatial resolution, because such plume-edge gradients are confined to a narrow frontal boundary whose width is scaled by the baroclinic Rossby radius of deformation (buoyancy-driven front), typically of order 5–20 km in theory in this subantarctic shelf region, far below the effective resolution of conventional merged altimetry products. Indeed, Ruiz Etcheverry et al. (2016) showed that ADT-derived geostrophic velocities over the Patagonian shelf at ∼54°S are weaker in austral winter (JJA) than in summer, because south of 42°S the annual sea level signal is dominated by thermosteric rather than halosteric effects at the large scales captured by gridded altimetry, meaning that the winter halosteric signature of the Magellan Plume, while dynamically significant at the frontal scale, is partially masked in large-scale ADT products by the background steric seasonality.

4.5 Remark on SST fronts not sensitive to ADT

Several fronts with above-threshold values in SST gradients do not show the same in the horizontal ADT gradients. Inspecting those fronts gives us a good insight into the dynamics of thermal fronts that have not yet been discussed. For example, fronts do not show an ADT signature, as they are rather subsurface, such as the Subtropical Shelf front (∼32°S, see e.g., Piola et al. (2010)), where cold Antarctic Shelf water and warm Brazil Shelf water meet, but freshwater from the Río de la Plata is overlaying its structure at the surface (Piola et al., 2000). Further, density differences do not always cause pressure gradients amplified enough to be visible in the horizontal gradients of ADT. Moreover, the stronger geostrophic velocities, and thus related ADT horizontal gradients, from the mean circulation on the SWACS overlap with possible smaller frontal signatures.
As an example, the Santa Cruz Coastal Front (∼47°S) is an estuarine plume front linked to the northern part of the (diluted) Magellan plume and local river discharge. While its dynamic is linked to tidal mixing and freshwater inflow, no frontal occurrence could be shown in ADT, when significant SST gradients were reached (e.g., see Appendix C3). Its limited expression in ADT may result from weak density gradients and its small spatial scale relative to the ADT product's resolution.

https://doi.org/10.5194/egusphere-2026-4751
Preprint. Discussion started: 13 August 2026

4.6 Is the Composite Front Detection applicable to SWOT L3?

The results presented above demonstrate that incorporating SWOT KaRIn swath data into the composite front detection framework substantially improves estimates of joint front probability, particularly in coastal and near-shelf regions where gridded altimetry products are known to smooth or suppress sharp gradients. This motivates a dedicated assessment of whether the composite method can be applied directly to the SWOT KaRIn Level-3 Expert product and whether doing so recovers frontal structures that remain undetected or underestimated in the gridded products compared in previous sections. To this end, the composite front detection method was applied to SWOT KaRIn Level-3 Expert data from the Cal/Val phase (2023-03-29 to 2023-07-09), which provided near-daily repeated coverage of Pass #007 across most of the study region over approximately 3 months. Adapting the method to wide-swath observations required three preprocessing steps: (1) gridded OSTIA SST fields were interpolated onto the KaRIn ADT sampling locations; (2) horizontal gradients in both ADT and SST were computed along the swath using finite differences between neighboring pixels; and (3) joint front probabilities were estimated using a spatial proximity criterion of approximately 10 km, which is consistent with the KaRIn pixel spacing and chosen to match the effective resolution of the swath data, rather than the single-grid-cell criterion (0.125°, approximately 14 km) used for the gridded products. The resulting time-mean fields are shown in Figure 11.

The magnitude of mean ADT gradient from KaRIn L3 (Figure 11a) is systematically higher than that from SWOT MIOST (Figure 11b) throughout the swath coverage. This contrast is most pronounced in three distinct coastal zones: the frontal region associated with the Magellan Strait outflow plume near 53-54°S, the Santa Cruz coastal zone between approximately 50–51°S, and the El Rincón area at the northern end of the domain near 40–41°S. This systematic suppression in the gridded product is consistent with the spatial low-pass filtering imposed by optimal interpolation, which broadens and attenuates sharp gradient features below the effective resolution of the correlation scales used in the mapping. The SST gradient field (Figure 11c) displays a complementary structure, with elevated values at the Magellan front and a broader, weaker gradient signature over the mid-shelf region, reflecting the coarser thermal contrast relative to the halinity-driven density front at the plume boundary. The resulting joint front probability on the KaRIn swath (Figure 11d) shows high P_{joint} values at two locations: the Magellan Strait plume front near 53°S, where probabilities approach 1.0, and in the El Rincón area near 41°S, where elevated probabilities extend further into the inner shelf than in the corresponding SWOT MIOST result (Figure 11e). The spatial extent of high-probability frontal occurrence is notably more confined and sharper in the KaRIn-based result, consistent with the higher gradient magnitudes recovered by the unsmoothed swath data. By contrast, the SWOT MIOST composite (Figure 11e) produces lower peak P_{joint} values and fails to detect the inner-shelf extension of the El Rincón front signal, suggesting that the gradient smoothing in the gridded product reduces simultaneous exceedance of both the ADT and SST thresholds required by the composite criterion. It is worth noting that the frontal signal near the Valdez Peninsula (~42.5°S) appears as a marginal high-ADT-gradient feature in panel (a) but does not emerge as a robust P_{joint} signal in panel (d).

While this analysis is necessarily limited by the availability of a single SWOT KaRIn track crossing the study region during the Cal/Val phase, it suggests that SWOT KaRIn Level-3 products may offer advantages over Level-4 maps for observing ocean fronts, highlighting their potential for further improvements in accuracy through the application of appropriate correc-

https://doi.org/10.5194/egusphere-2026-4751
Preprint. Discussion started: 13 August 2026

tions over the SWACS (Cornejo-Guzmán et al., 2026). This result is particularly encouraging in the context of the upcoming Sentinel-3 Next Generation Topography mission, whose planned constellation of two wide-swath interferometric altimeters will substantially improve the spatial and temporal coverage of Level-3 observations.

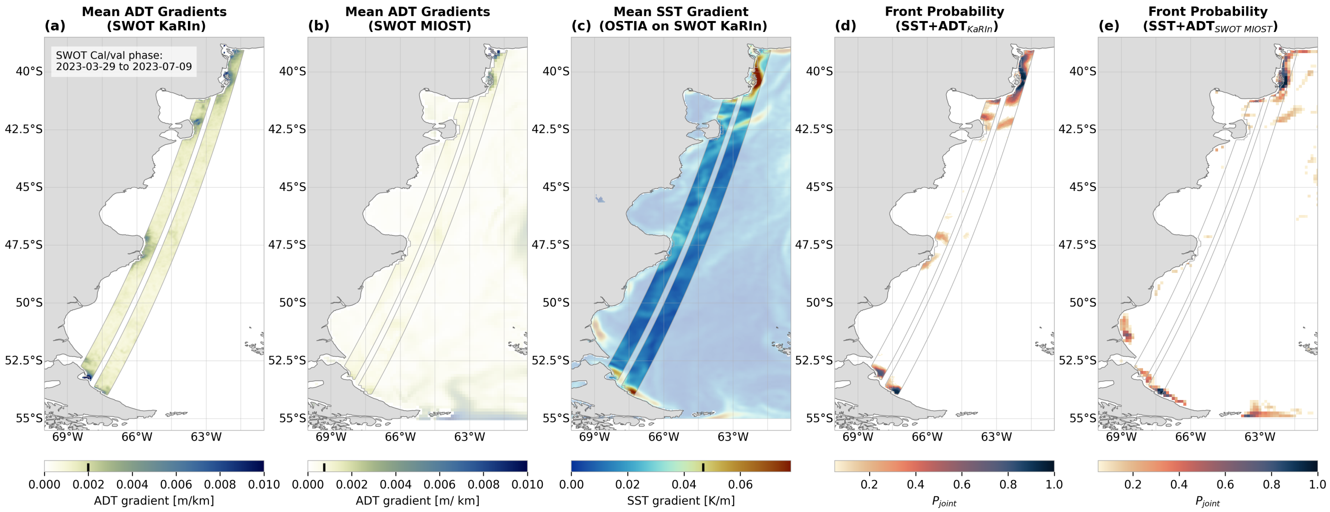

Figure 11. Composite Front Detection using SWOT Cal/val phase: mean horizontal gradients in ADT from SWOT KaRIn L3 Expert (a) and SWOT MIOST (b), mean horizontal gradients in SST (c), and resulting front probabilities using ADTs from SWOT KaRIn Expert (d) and SWOT MIOST (e). Threshold for individual front criteria following the percentiles marked in the colorbar.

https://doi.org/10.5194/egusphere-2026-4751
Preprint. Discussion started: 13 August 2026

5 Conclusion

In this study, we introduced a composite front detection framework combining horizontal gradient thresholds applied simultaneously to Sea Surface Temperature (SST) and Absolute Dynamic Topography (ADT) to identify dynamically active frontal structures on the Southwestern Atlantic Continental Shelf (SWACS). By applying this method to four ADT datasets, CMEMS MIOST, the SWOT-enhanced SWOT MIOST, the regional OK-STv2 product, and the GLORYS12v1 model reanalysis, over a one-year period from July 2023 to July 2024, we evaluated which front types produce detectable ADT gradient signatures and how well different products resolve them.

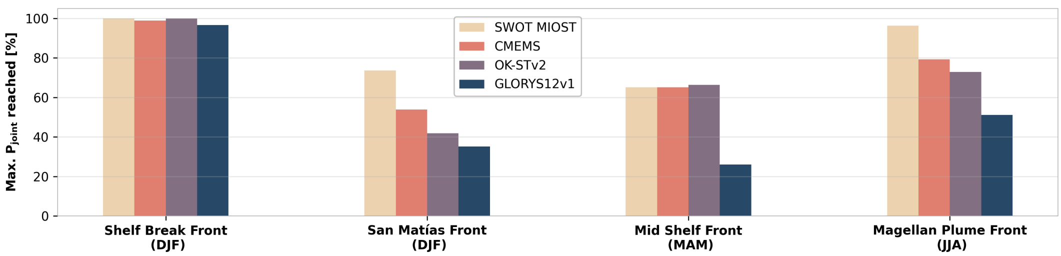

Figure 12. Summary of maximal front probabilities (P_{joint}) at different fronts detected in distinct seasons (brackets), using different ADT datasets.

The method identified frontal structures at well-established locations across the SWACS, suggesting that high front probabilities (P_{joint}) are confined to dynamically meaningful regions. The permanent Patagonian Shelf-Break Front is robustly detected by all datasets, reaching 100% P_{joint} in austral summer (DJF) between 40° and 44°S, consistent with the known intensification of the front during the period of maximum shelf stratification (Piola et al., 2010). This result supports the composite approach and indicates that large-scale, bathymetrically constrained fronts with strong geostrophic expression are consistently detectable across all ADT products.

Moving to more complex coastal and seasonal fronts, dataset differences become more pronounced and diagnostically informative. The San Matías Gulf tidal mixing front, a seasonal and coastal front that forms in austral summer at the interface between tidally mixed and stratified waters, illustrates the limits of conventional gridded altimetry in coastal regions. While SWOT MIOST clearly identifies this front with P_{joint} reaching 73.63%, conventional nadir-only products (CMEMS: 54.95%; OK-STv2: 41.86%) only partially detect it, while GLORYS12v1 reaches only 35.16%, which is likely connected to the missing tides in the model. Thus, tidal mixing might not be correctly represented in Glorys12v1 numerical model (Lellouche et al., 2018). The differences between the observational and model datasets are likely linked to the model exhibiting the largest RMSE relative to altimetry in coastal, shelf, and sharp-front areas, as shown in Lellouche et al. (2021). These results at the San Matías Front demonstrate that the addition of SWOT KaRIn observations resolves ADT gradients at the coastal scales necessary to co-detect shallow mixing fronts, representing a qualitative capability advance over nadir-only altimetry in complex gulf environments.

https://doi.org/10.5194/egusphere-2026-4751
Preprint. Discussion started: 13 August 2026

The Mid-Shelf Front at 39 to 40°S presents a contrasting picture: all altimetry-based datasets achieve >65% P_{joint} in MAM, confirming that this front produces ADT gradients at scales well above the effective resolution limits of conventional altimetry. Its year-round ADT signature and MAM-specific SST expression reflect the seasonal sharpening of the thermohaline water mass boundary between San Matías Gulf waters and Patagonian Current shelf waters, which simultaneously satisfies both gradient thresholds of the composite detection during austral autumn. Here, SWOT MIOST's contribution is not detection but spatial sharpness: it produces a more localized and coherent cross-shelf frontal peak in the transect analysis, better resolving the along-front geostrophic jet documented in the literature (Strub et al., 2015; Ruiz Etcheverry et al., 2016). Further, the composite front detection framework was applied to SWOT KaRIn Level 3 Expert data during the Cal/Val phase to evaluate its flexibility across different altimetry products and its potential for resolving frontal structures. Compared with the corresponding SWOT MIOST product, SWOT KaRIn Level 3 exhibits enhanced ADT gradients, particularly across narrow coastal frontal regions. This indicates that the reduced spatial smoothing of wide-swath SWOT observations may improve the representation of sharp frontal gradients that are attenuated in gridded Level 4 products. Despite the test being limited by the short Cal/Val sampling period and the availability of a single SWOT track, this application demonstrates the adaptability of the composite front detection and highlights its potential for exploiting future wide-swath observations.

Taken together, these results establish a hierarchy of front detectability through composite SST+ADT detection as a function of the dominant frontal mechanism and spatial scale. Large-scale, bathymetrically steered, thermohaline fronts with strong geostrophic expression are robustly detectable by all products. Coastal tidal mixing fronts and narrow buoyancy-driven plume fronts, whose ADT gradients operate at scales below the effective resolution of conventional altimetry ($\sim$100 km; see Ballarotta et al. (2019)), benefit most from SWOT-enhanced gridded products. Fronts whose density contrast does not generate a sufficiently strong geostrophic ADT gradient relative to the background large-scale ADT field, such as the Subtropical Shelf Front, remain undetectable by the composite approach regardless of product resolution, highlighting a key limitation of the SST+ADT framework for thermohaline fronts in strong background circulation.

Future work should extend this analysis to longer time series as SWOT MIOST data accumulate, examine the impact of ADT effective resolution on detection thresholds more systematically, and explore whether the composite framework can be adapted to fronts with weak ADT signatures by conditioning on seasonal or spatial subsets of the ADT gradient fields. To further assess the impact of SWOT KaRIn observations on the representation of shelf dynamics, future studies should evaluate model simulations that assimilate SWOT KaRIn data, as suggested in Fouchet et al. (2025). Such analyses could determine whether SWOT's enhanced spatial resolution improves the model's ability to detect and represent shelf fronts. Additionally, the composite framework developed here could be extended to other gridded remote-sensing products, such as ocean color observations, potentially revealing additional physical and biogeochemical linkages associated with shelf-front variability.

Code and data availability. Sample code for computing the joint front probability in the study region is available under https://github.com/mariejuhl/Composite_Front_Detection.

This study has been conducted using E.U. Copernicus Marine Service Information, such as the Sea Surface Temperatures from the Operational Sea Surface Temperature and Ice Analysis (OSTIA, https://doi.org/10.48670/moi-00165, accessed February 2026), the global gridded altimetry ADTs from the product (https://doi.org/10.48670/moi-00148, accessed January 2026) and the numerical model reanalysis GLORYS12v1 (https://doi.org/10.48670/moi-00021). The SWOT MIOST gridded data are published as “Experimental multimission gridded L4 sea level heights and velocities with SWOT" product on AVISO (https://doi.org/10.24400/527896/A01-2024.007 (v2.0.1), accessed March 2026). The OK-STv2 regional data are available on SEANOE (https://www.seanoe.org/data/00928/103947/).

https://doi.org/10.5194/egusphere-2026-4751
Preprint. Discussion started: 13 August 2026

Appendix A: Seasonality ADT Thresholds

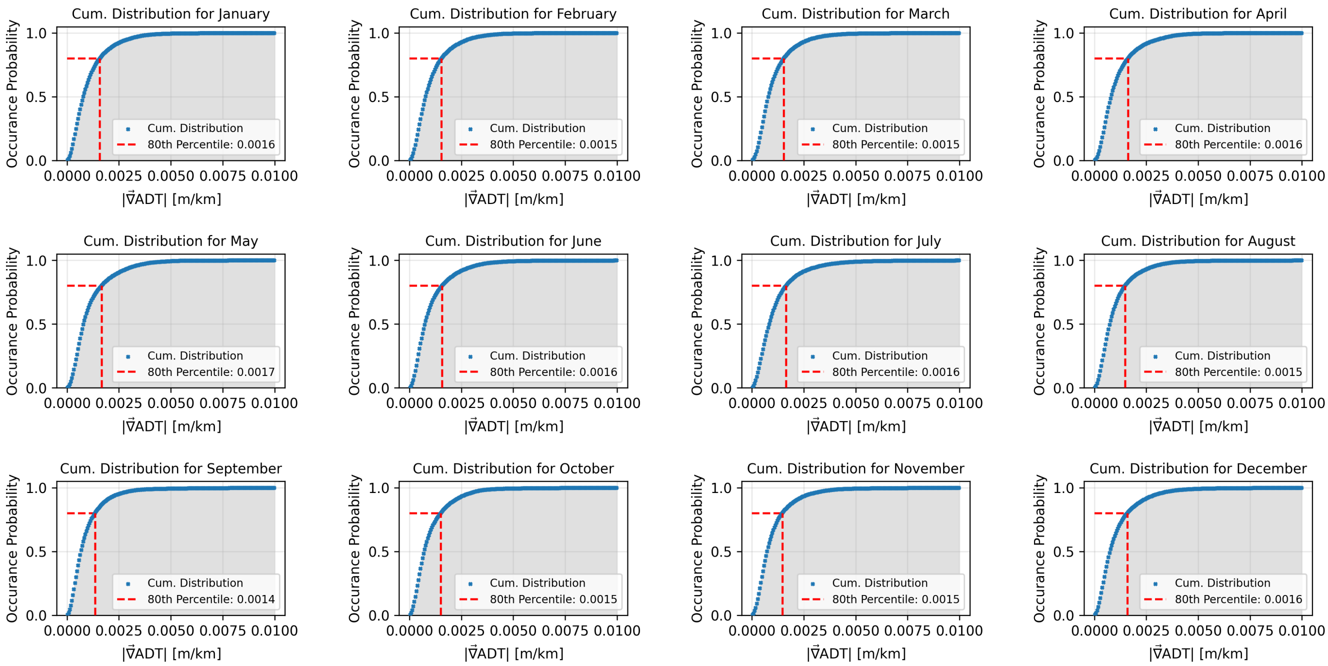

Figure A1. Monthly cumulative density distribution of horizontal gradients of ADT from SWOT MIOST. 80th percentile marked with a red line.

https://doi.org/10.5194/egusphere-2026-4751
Preprint. Discussion started: 13 August 2026

Appendix B: Sensitivity to ADT thresholds

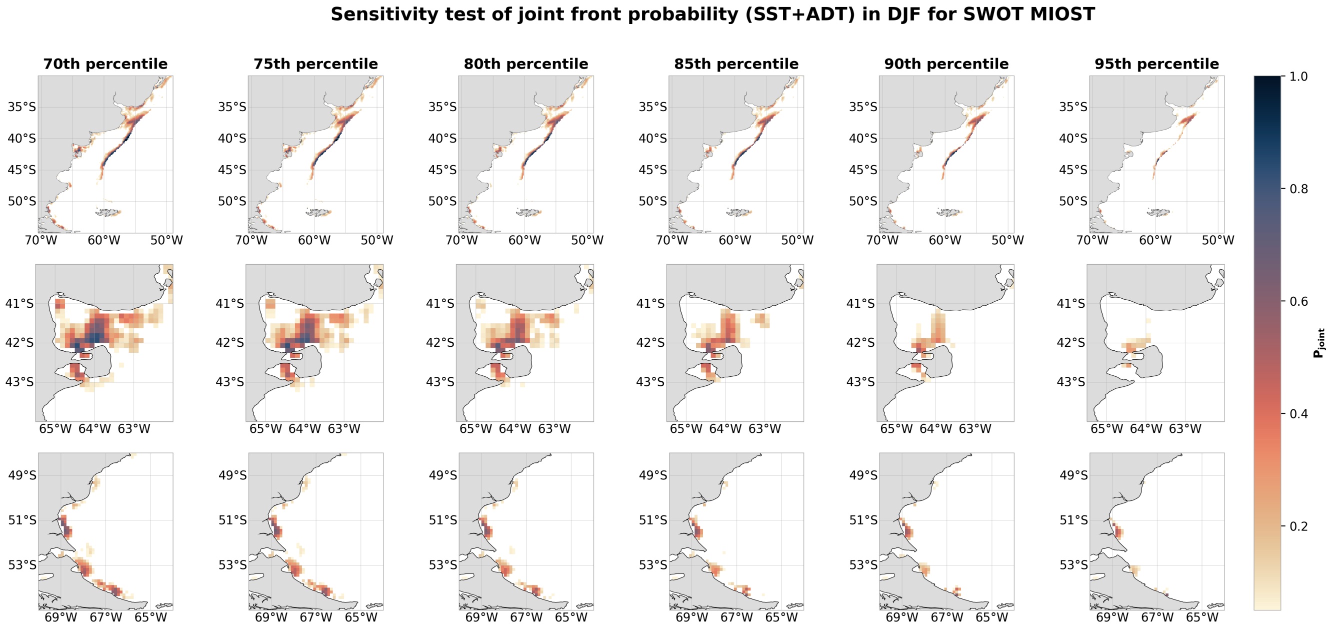

Figure B1. Sensitivity of joint front probability to percentiles of the ADT threshold in season DJF shown for the whole SWACS (top) and the San Matías Front (bottom).

https://doi.org/10.5194/egusphere-2026-4751
Preprint. Discussion started: 13 August 2026

Appendix C: Monthly horizontal Gradients

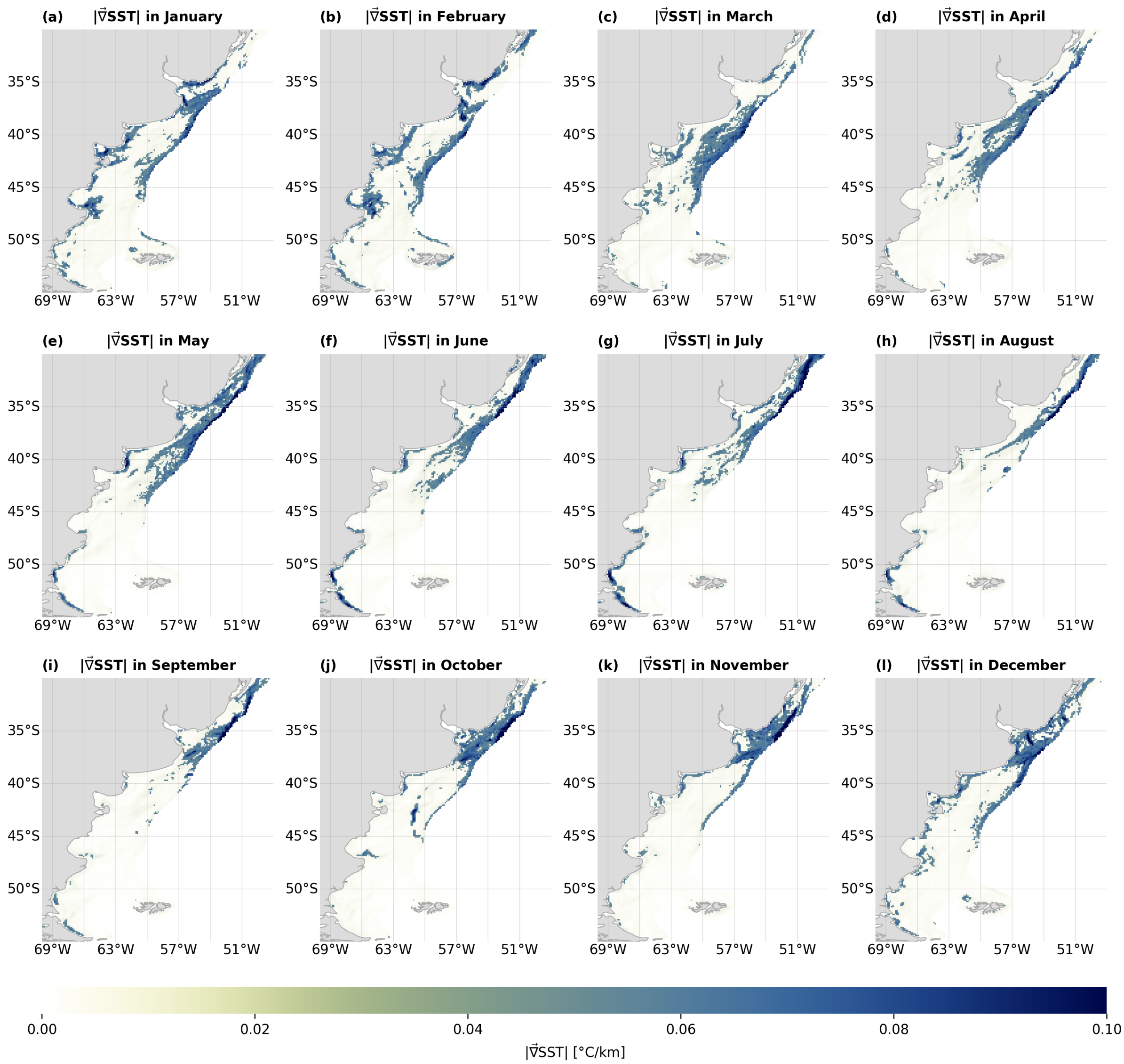

Figure C1. Monthly mean horizontal gradients of SST in °C/km per grid point. Gradients below the threshold for an SST front are semi-transparent.

https://doi.org/10.5194/egusphere-2026-4751
Preprint. Discussion started: 13 August 2026

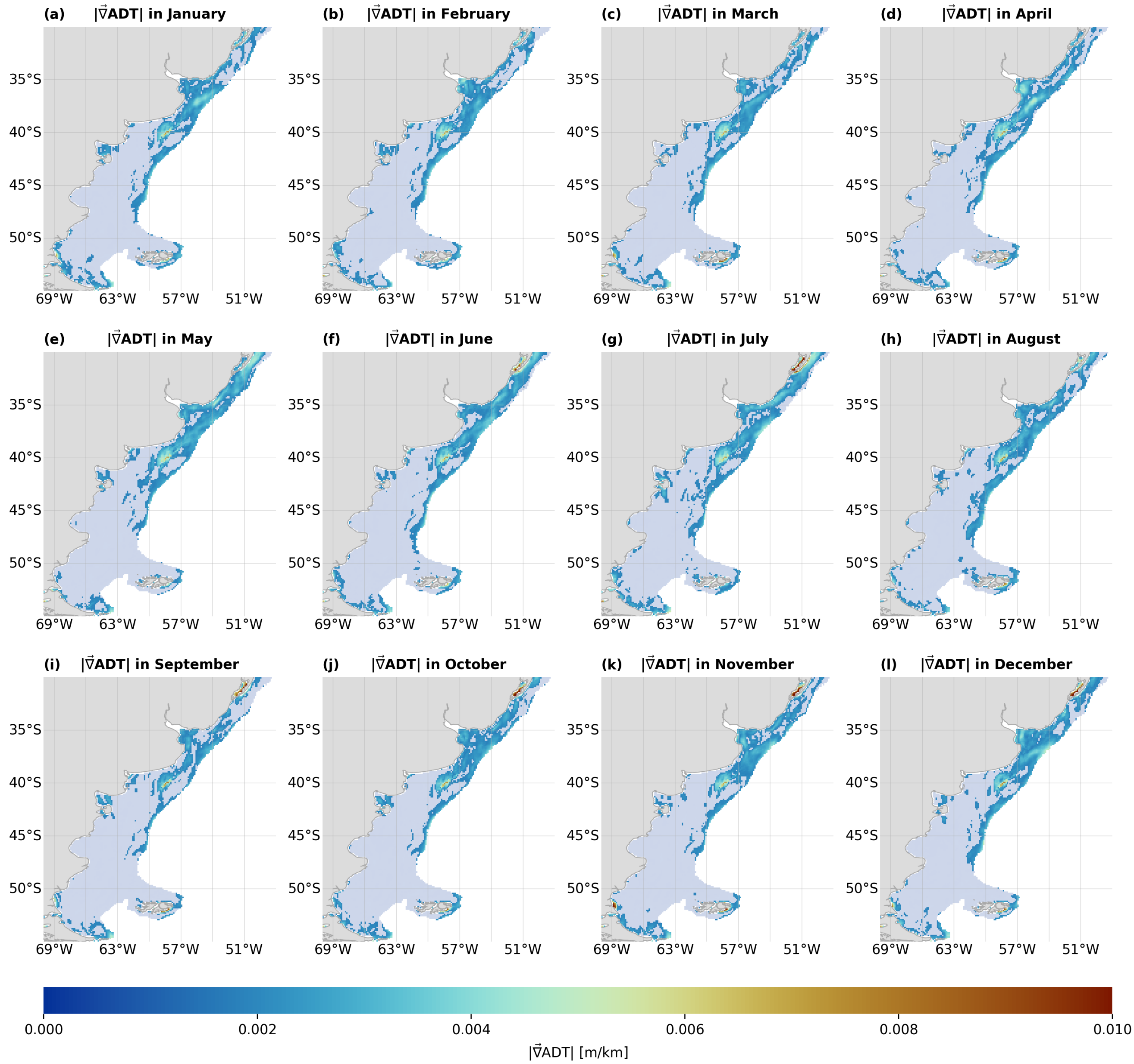

Figure C2. Monthly mean horizontal gradients of ADT from SWOT MIOST in m/km per grid point. Gradients below the threshold for an ADT front are semi-transparent.

https://doi.org/10.5194/egusphere-2026-4751
Preprint. Discussion started: 13 August 2026

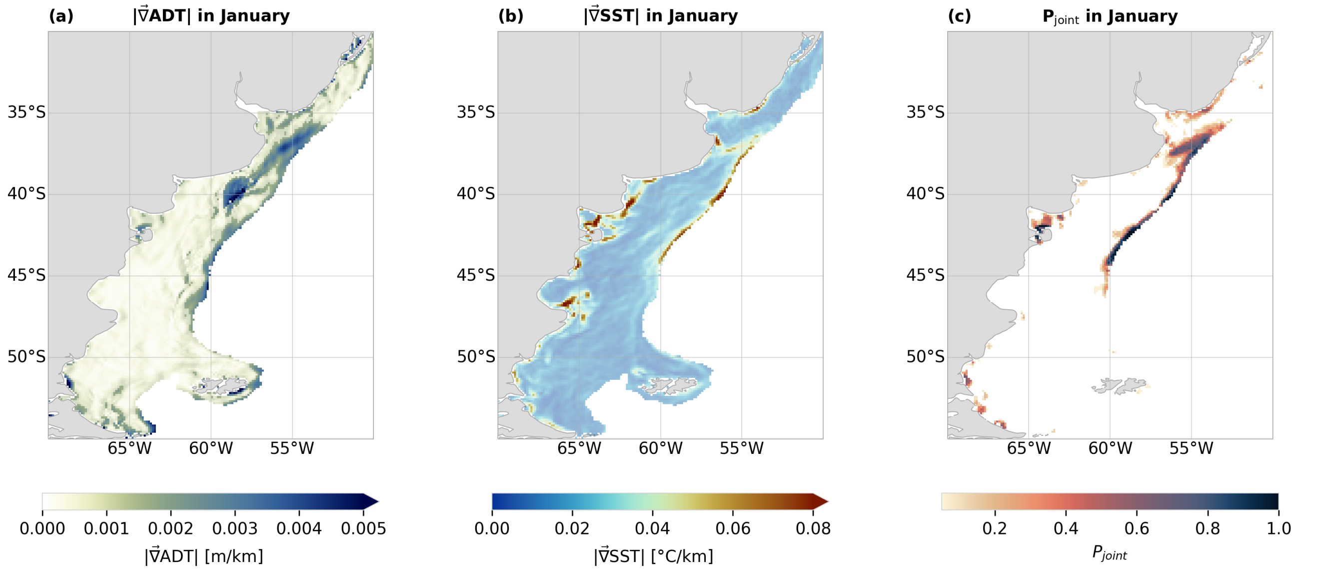

Figure C3. Monthly mean horizontal gradients in January of ADT from SWOT MIOST in m/km (a), SST from OSTIA in °C/km (b), and resulting joint front probability for January (c).

https://doi.org/10.5194/egusphere-2026-4751
Preprint. Discussion started: 13 August 2026

445 ## Appendix D: Seasonal SST

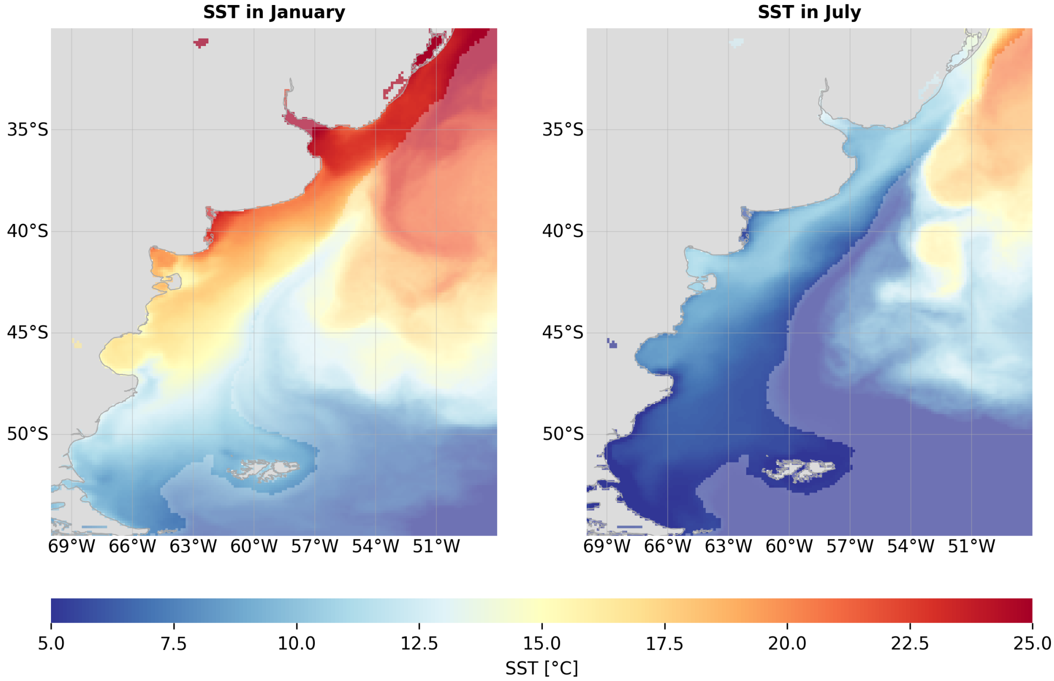

Figure D1. Monthly mean SST from OSTIA for January and July in the study period. Regions outside the continental shelf (200m-isobath) are semi-transparent.

Author contributions. MCJ conceived this study and produced the results of the manuscript. All co-authors provided input on the methods, contributed to the analysis/interpretation of the results, and contributed to the writing of the manuscript.

Competing interests. The contact author has declared that none of the authors has any competing interests.

Acknowledgements. The OK-STv2 reprocessing and SWOT data storage were made possible by hardware funded through the European
450 Space Agency's Earth Observation Excellence Award (M. Passaro, Individual Winner 2025).

https://doi.org/10.5194/egusphere-2026-4751
Preprint. Discussion started: 13 August 2026

References

Acha, E. M., Mianzan, H. W., Guerrero, R. A., Favero, M., and Bava, J.: Marine fronts at the continental shelves of austral South America: physical and ecological processes, Journal of Marine systems, 44, 83–105, 2004.

Archer, M., Wang, J., Klein, P., Dibarboure, G., and Fu, L.-L.: Wide-swath satellite altimetry unveils global submesoscale ocean dynamics, Nature, 640, 691–696, https://doi.org/10.1038/s41586-025-08722-8, 2025.

Artana, C., Provost, C., Lellouche, J.-M., Rio, M.-H., Ferrari, R., and Sennéchael, N.: The Malvinas current at the confluence with the Brazil current: Inferences from 25 years of Mercator ocean reanalysis, Journal of Geophysical Research: Oceans, 124, 7178–7200, 2019.

Ballarotta, M., Ubelmann, C., Pujol, M.-I., Taburet, G., Fournier, F., Legeais, J.-F., Faugère, Y., Delepoulle, A., Chelton, D., Dibarboure, G., et al.: On the resolutions of ocean altimetry maps, Ocean science, 15, 1091–1109, 2019.

Barclay, V. M., Neill, S. P., and Angeloudis, A.: Tidal range resource of the Patagonian shelf, Renewable Energy, 209, 85–96, 2023.

Belkin, I. M.: Remote sensing of ocean fronts in marine ecology and fisheries, Remote sensing, 13, 883, 2021.

Belkin, I. M., Cornillon, P. C., and Sherman, K.: Fronts in large marine ecosystems, Progress in Oceanography, 81, 223–236, 2009.

Brink, K.: Cross-shelf exchange, Annual review of marine science, 8, 59–78, 2016.

Brun, A. A., Ramirez, N., Pizarro, O., and Piola, A. R.: The role of the Magellan Strait on the southwest South Atlantic shelf, Estuarine, Coastal and Shelf Science, 237, 106 661, 2020.

Burrage, D., Wesson, J., Martinez, C., Pérez, T., Möller Jr, O., and Piola, A.: Patos Lagoon outflow within the Río de la Plata plume using an airborne salinity mapper: Observing an embedded plume, Continental Shelf Research, 28, 1625–1638, 2008.

Canny, J.: A computational approach to edge detection, IEEE Transactions on pattern analysis and machine intelligence, pp. 679–698, 2009.

Cayula, J.-F. and Cornillon, P.: Edge detection algorithm for SST images, Journal of atmospheric and oceanic technology, 9, 67–80, 1992.

Chambers, D. P.: Using kinetic energy measurements from altimetry to detect shifts in the positions of fronts in the Southern Ocean, Ocean Science, 14, 105–116, 2018.

Cornejo-Guzmán, S., Saraceno, M., Ruiz-Etcheverry, L. A., Birol, F., and Lyard, F.: On the Accuracy of SWOT Sea Surface Height Over Large Continental Shelves, 2026.

Donlon, C. J., Martin, M., Stark, J., Roberts-Jones, J., Fiedler, E., and Wimmer, W.: The operational sea surface temperature and sea ice analysis (OSTIA) system, Remote sensing of Environment, 116, 140–158, 2012.

Fouchet, E., Benkiran, M., Le Traon, P.-Y., and Remy, E.: Comparison of a global high-resolution ocean data assimilation system with SWOT observations, Frontiers in Marine Science, Volume 12 - 2025, https://doi.org/10.3389/fmars.2025.1563934, 2025.

Franco, B. C., Palma, E. D., Combes, V., and Lasta, M. L.: Physical processes controlling passive larval transport at the Patagonian Shelf Break Front, Journal of Sea Research, 124, 17–25, 2017.

Fu, L.-L., Pavelsky, T., Morrow, R., Cretaux, J.-F., and Farrar, T.: The SWOT (surface water and ocean topography) mission and its status, in: EGU General Assembly Conference Abstracts, pp. EGU–17 156, 2023.

Graham, R. M.: The location and variability of Southern Ocean fronts, Ph.D. thesis, Stockholms universitets förlag, 2013.

Hart-Davis, M. G., Sulzbach, R., Talke, S. A., Haigh, I. D., Marcos, M., Woodworth, P., Ray, R., Andersen, O. B., Lyard, F., Fouchet, E., et al.: Tide of the Time: Global tidal characteristics observed from in-situ measurements, Ocean Science, 22, 1681–1709, 2026.

Huthnance, J. M.: Circulation, exchange and water masses at the ocean margin: the role of physical processes at the shelf edge, Progress in Oceanography, 35, 353–431, 1995.

Juhl, M.-C., Passaro, M., Dettmering, D., and Saraceno, M.: Evaluation of the sub-annual sea level anomalies in the continental shelf of the Southwestern Atlantic and their relation to wind variability, Ocean Dynamics, 74, 595–612, 2024.

Juhl, M.-C., Passaro, M., and Dettmering, D.: Regional daily sea level maps from Multi-mission Altimetry using Space–time Window Kriging, Advances in Space Research, 2025.

Juhl, M.-C., Passaro, M., and Dettmering, D.: Daily Gridded Sea Level Anomalies from Satellite Altimetry Using Spatio Temporal Window Kriging, https://doi.org/10.17882/103947, 2026.

Lago, L. S., Saraceno, M., Martos, P., Guerrero, R. A., Piola, A. R., Paniagua, G. F., Ferrari, R., Artana, C. I., and Provost, C.: On the Wind Contribution to the Variability of Ocean Currents Over Wide Continental Shelves: A Case Study on the Northern Argentine Continental Shelf, Journal of Geophysical Research: Oceans, 124, 7457–7472, https://doi.org/10.1029/2019JC015105, 2019.

Lago, L. S., Saraceno, M., Piola, A. R., and Ruiz-Etcheverry, L. A.: Volume transport variability on the northern argentine continental shelf from in situ and satellite altimetry data, Journal of Geophysical Research: Oceans, 126, e2020JC016 813, 2021.

Lellouche, J.-M., Greiner, E., Le Galloudec, O., Garric, G., Regnier, C., Drevillon, M., Benkiran, M., Testut, C.-E., Bourdalle-Badie, R., Gasparin, F., et al.: Recent updates to the Copernicus Marine Service global ocean monitoring and forecasting real-time 1/ 12 high-resolution system, Ocean Science, 14, 1093–1126, 2018.

Lellouche, J.-M., Greiner, E., Bourdallé-Badie, R., Garric, G., Melet, A., Drévillon, M., Bricaud, C., Hamon, M., Le Galloudec, O., Regnier, C., Candela, T., Testut, C.-E., Gasparin, F., Ruggiero, G., Benkiran, M., Drillet, Y., and Pierre-Yves, L. T.: The Copernicus Global 1/12° Oceanic and Sea Ice GLORYS12 Reanalysis, Frontiers in Earth Science, Volume 9 - 2021, https://doi.org/10.3389/feart.2021.698876, 2021.

Lucas, A. J., Guerrero, R. A., Mianzan, H. W., Acha, E. M., and Lasta, C. A.: Coastal oceanographic regimes of the northern Argentine continental shelf (34–43 S), Estuarine, Coastal and Shelf Science, 65, 405–420, 2005.

Marrari, M., Signorini, S. R., McClain, C. R., Pájaro, M., Martos, P., Viñas, M. D., Hansen, J., Dimauro, R., Cepeda, G., and Buratti, C.: Reproductive success of the Argentine anchovy, Engraulis anchoita, in relation to environmental variability at a mid-shelf front (Southwestern Atlantic Ocean), Fisheries Oceanography, 22, 247–261, https://doi.org/10.1111/fog.12019, 2013.

Miller, P.: Composite front maps for improved visibility of dynamic sea-surface features on cloudy SeaWiFS and AVHRR data, Journal of Marine systems, 78, 327–336, 2009.

Nieto, K., Demarcq, H., and McClatchie, S.: Mesoscale frontal structures in the Canary Upwelling System: New front and filament detection algorithms applied to spatial and temporal patterns, Remote Sensing of Environment, 123, 339–346, https://doi.org/10.1016/j.rse.2012.03.028, 2012.

Palma, E. D. and Matano, R. P.: A numerical study of the Magellan Plume, Journal of Geophysical Research: Oceans, 117, 2012.

Passaro, M.: Can satellite altimetry observe coastally trapped waves on sub-monthly timescales?, Ocean Science, 21, 2663–2679, 2025.

Piola, A. R., Campos, E. J., Möller Jr, O. O., Charo, M., and Martinez, C.: Subtropical shelf front off eastern South America, Journal of Geophysical Research: Oceans, 105, 6565–6578, 2000.

Piola, A. R., Matano, R. P., Palma, E. D., Möller Jr, O. O., and Campos, E. J.: The influence of the Plata River discharge on the western South Atlantic shelf, Geophysical Research Letters, 32, 2005.

Piola, A. R., Martínez Avellaneda, N., Guerrero, R. A., Jardón, F. P., Palma, E. D., and Romero, S. I.: Malvinas-slope water intrusions on the northern Patagonia continental shelf, Ocean Science, 6, 345–359, https://doi.org/10.5194/os-6-345-2010, 2010.

Pisoni, J. P., Rivas, A. L., and Piola, A. R.: On the variability of tidal fronts on a macrotidal continental shelf, Northern Patagonia, Argentina, Deep Sea Research Part II: Topical Studies in Oceanography, 119, 61–68, 2015.

https://doi.org/10.5194/egusphere-2026-4751
Preprint. Discussion started: 13 August 2026

Poli, L., Artana, C., Provost, C., and Le Dissez, A.: First insights from SWOT fast sampling phase: High frequency coastal trapped waves over the Patagonian shelf, Geophysical Research Letters, 52, e2024GL112 506, 2025.

Rivas, A. L.: Quantitative estimation of the influence of surface thermal fronts over chlorophyll concentration at the Patagonian shelf, Journal of Marine Systems, 63, 183–190, 2006.

Rivas, A. L. and Pisoni, J. P.: Identification, characteristics and seasonal evolution of surface thermal fronts in the Argentinean Continental Shelf, Journal of Marine Systems, 79, 134–143, 2010.

Ruiz Etcheverry, L. A., Saraceno, M., Piola, A. R., and Strub, P. T.: Sea level anomaly on the Patagonian continental shelf: Trends, annual patterns and geostrophic flows, Journal of Geophysical Research: Oceans, 121, 2733–2754, https://doi.org/https://doi.org/10.1002/2015JC011265, 2016.

Saraceno, M., Provost, C., Piola, A. R., Bava, J., and Gagliardini, A.: Brazil Malvinas Frontal System as seen from 9 years of advanced very high resolution radiometer data, Journal of Geophysical Research: Oceans, 109, 2004.

Saraceno, M., Simionato, C. G., and Ruiz-Etcheverry, L. A.: Sea surface height trend and variability at seasonal and interannual time scales in the Southeastern South American continental shelf between 27 S and 40 S, Continental Shelf Research, 91, 82–94, 2014.

Sharples, J.: Potential impacts of the spring-neap tidal cycle on shelf sea primary production, Journal of Plankton Research, 30, 183–197, 2008.

Siegelman, L., Klein, P., Thompson, A. F., Torres, H. S., and Menemenlis, D.: Altimetry-based diagnosis of deep-reaching sub-mesoscale ocean fronts, Fluids, 5, 145, 2020.

Simpson, J. H. and Hunter, J.: Fronts in the Irish sea, Nature, 250, 404–406, 1974.

Simpson, J. H. and Sharples, J.: Introduction to the physical and biological oceanography of shelf seas, Cambridge University Press, 2012.

Sokolov, S. and Rintoul, S. R.: Circumpolar structure and distribution of the Antarctic Circumpolar Current fronts: 1. Mean circumpolar paths, Journal of Geophysical Research: Oceans, 114, 2009.

Strub, P. T., James, C., Combes, V., Matano, R. P., Piola, A. R., Palma, E. D., Saraceno, M., Guerrero, R. A., Fenco, H., and Ruiz-Etcheverry, L. A.: Altimeter-derived seasonal circulation on the southwest Atlantic shelf: 27°–43° S, Journal of Geophysical Research: Oceans, 120, 3391–3418, 2015.

Sudre, F., Hernández-Carrasco, I., Mazoyer, C., Sudre, J., Dewitte, B., Garçon, V., and Rossi, V.: An ocean front dataset for the Mediterranean sea and southwest Indian ocean, Scientific Data, 10, 730, 2023.

Ubelmann, C., Carrere, L., Durand, C., Dibarboure, G., Faugère, Y., Ballarotta, M., Briol, F., and Lyard, F.: Simultaneous estimation of ocean mesoscale and coherent internal tide sea surface height signatures from the global altimetry record, Ocean Science Discussions, 2021, 1–19, 2021a.

Ubelmann, C., Dibarboure, G., Gaultier, L., Ponte, A., Ardhuin, F., Ballarotta, M., and Faugère, Y.: Reconstructing ocean surface current combining altimetry and future spaceborne Doppler data, Journal of Geophysical Research: Oceans, 126, e2020JC016 560, 2021b.

Verger-Miralles, E., Mourre, B., Gómez-Navarro, L., Barceló-Llull, B., Casas, B., Cutolo, E., Díaz-Barroso, L., d'Ovidio, F., Tarry, D. R., Zarokanellos, N. D., and Pascual, A.: SWOT Enhances Small-Scale Eddy Detection in the Mediterranean Sea, Geophysical Research Letters, 52, e2025GL116 480, https://doi.org/10.1029/2025GL116480, 2025.

Wang, Z., Chen, G., Han, Y., Ma, C., and Lv, M.: Southwestern Atlantic Ocean fronts detected from satellite-derived SST and chlorophyll, Remote Sensing, 13, 4402, 2021.